Understanding THz Pulse Propagation in the Atmosphere

Yihong Yang, *Student Member, IEEE*, Mahboubeh Mandehgar, and Daniel R. Grischkowsky, *Fellow, IEEE*

***Abstract*—In this paper, we have extracted the THz refractivity of water vapor $(n(\omega) - 1)$ from the complex spectra of the precise coherent THz-TDS absorption measurement with a 6.18 m long sample path [1]. We fit the new refractivity and the previous absorption measurements to the sum of the contributions from all of the water vapor lines (with the same van-Vleck Weisskopf lineshape) in the JPL, Pasadena, CA, database from 0 to 10 THz. The precision of the resulting theoretical absorption and refractivity is demonstrated by the good agreement between the calculated THz output pulse and the measured output pulse, both having the same THz input pulse.**

Using this capability, we have calculated the transmitted THz pulses through the atmosphere at specified humidity and temperature for a variety of input pulses for the distances of 500, 1000, and 2000 m. We have also tested the predicted stable propagation of the proposed "ideal THz bit pulse" [2], and showed that this pulse evolves into two overlapping pulses after 2000 m of propagation. We showed these two new pulses I and II to be transform-limited THz bit pulses with stable propagation to 2000 m. THz bit pulses I and II span the spectral ranges of 0.13–0.18 THz and 0.18–0.33 THz, respectively, and can support the bit rate distance products of 20 and 40 (Gb/s)·km, respectively.

***Index Terms*—Absorption, atmospheric transmission, spectroscopy, terahertz (THz), THz communication.**

I. Introduction

In THE FREQUENCY range 0.1–10 THz, the frequency-dependent absorption $\alpha(\omega)$ and the corresponding dispersive index of refraction $n(\omega)$ of water vapor control the electromagnetic propagation of broad-bandwidth THz pulses and narrow-band THz waves in the atmosphere. Because the index $n(\omega)$ is quite small, the refractivity term $[n(\omega) - 1]$ is usually discussed. The strong absorption by water vapor determines the maximum propagation distance of THz waves in the atmosphere, while the reshaping of propagating broad-bandwidth short THz pulses is equally controlled by both the refractivity $[n(\omega) - 1]$ and the absorption $\alpha(\omega)$. Overviews of the earlier work involving measurements of the absorption $\alpha(\omega)$ of water vapor in the atmosphere are presented in [1]–[3].

In this paper, we first use the previous coherent THz time-domain spectroscopy (THz-TDS) measurements of $\alpha(\omega)$ for water vapor [1], to determine the corresponding $[n(\omega) - 1]$. These earlier amplitude and phase THz-TDS measurements were originally only analyzed for the amplitude absorption and were not compared to theory. We then use the numerically fit, analytic and causal van-Vleck Weisskopf (v-VW) lineshape functions [4], [5] for $\alpha(\omega)$ and the corresponding $[n(\omega) - 1]$ to calculate THz pulse propagation in the frequency domain. Then, by IFFT we obtain the time domain output pulses, in good agreement with the measured pulses.

Using this capability, we calculate the transmitted THz pulses through the atmosphere at specified humidity and temperature for the extended distances of 250, 500, 1000 and 2000 m using previous long-path measurements [2], as input pulses. Based on our calculation's close connection to experiment, the calculated results relate to actual measurement capabilities and provide expected signal to noise predictions. We also test the predicted stable propagation of the proposed "ideal THz bit pulse" [2], and show that this pulse evolves into two overlapping pulses after 1000 m of propagation. These two pulses I and II are shown to be transform-limited THz bit pulses with stable propagation to 2000 m. THz bit pulse I and II span the spectral ranges of 0.13–0.18 THz and 0.18–0.33 THz, respectively, and can support the bit rate distance products of 20 (Gb/s)-km, and 40 (Gb/s)-km, respectively. These results are very competitive with optical fiber digital communications channels, and clearly show the potential for many applications.

II. Discussion of the Previous Long-Tube THz-TDS Measurement of the Atmosphere

We will now discuss the previous precise coherent THz-TDS measurement of a 6.18 m path of the atmosphere at 21°C and relative humidity (RH) 51% [1], where the technical details of the measurement are presented. From these measurements, we will extract the refractivity $(n(\omega) - 1)$ of water vapor. For THz-TDS two measurements of the transmitted electric field pulse are measured, the reference pulse with no sample in place and the sample pulse with the sample in place. Then, if all the other measurement details remained the same, the ratios of the corresponding amplitude Fourier transforms (amplitude spectra) gives the amplitude transmission of the sample. This is illustrated in Fig. 1(a), where the bottom trace is the measured reference pulse with dry air at less than 0.5% RH in the sample chamber, and the top trace is the measured sample pulse with the sample chamber filled with air and water vapor at RH 51%. Fig. 1(b) shows the corresponding amplitude Fourier transforms (amplitude spectra) of these pulses, where the upper spectrum is that of the reference pulse and the lower spectrum is that of the sample pulse.

As shown in Fig. 1, the reference and sample pulses were measured over a scan duration of 165 ps, corresponding to the frequency resolution of 6.1 GHz. For a complete experimental

Manuscript received April 23, 2012; revised May 25, 2012; accepted May 30, 2012. Date of publication June 29, 2012; date of current version July 12, 2012. This work was supported in part by the DTRA (10-2960M), the Air Force Research Laboratory (AFRL) and the National Science Foundation.

The authors are with the School of Electrical and Computer Engineering, Oklahoma State University, Stillwater, OK 74078, USA (e-mail: daniel.grischkowsky@okstate.edu).

Color versions of one or more of the figures in this paper are available online at http://ieeexplore.ieee.org.

Digital Object Identifier 10.1109/TTHZ.2012.2203429

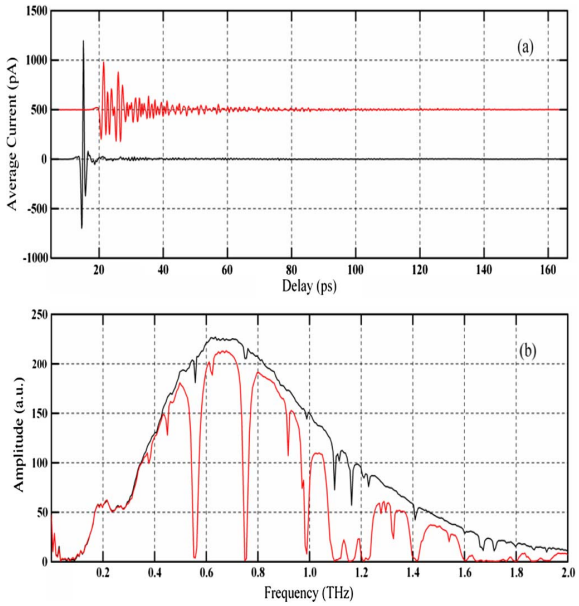

Fig. 1. (a) Measured THz reference pulse (lower trace) and measured THz sample pulse (upper trace). (b) Corresponding amplitude spectrum (upper curve) for the THz reference pulse and for the sample pulse (lower curve). (Figure adapted from [1].)

measurement series, 4 reference dry-air pulses and 4 sample humid-air pulses were measured. The reference pulse shows little oscillation due to the small amount of water vapor remaining in the sample chamber. When the sample chamber was filled with laboratory air with RH 51% at 21 °C, the sample pulse showed very strong and extended ringing from the rotational lines of water vapor.

During the later data analysis, the individual reference and sample pulses were zero-padded to a total scan length of 1650 ps. The amplitude spectra of these zero-padded pulses were obtained from their numerical complex Fourier transforms and were then averaged to obtain the final amplitude spectra shown in Fig. 1(b). The reference spectrum weakly shows the strong water lines, indicating that the residual water vapor in the sample space was less than RH 0.5%. In contrast, the sample spectrum shows complete absorption for the strong water lines.

The amplitude transmission shown in Fig. 2 is simply the ratio of the sample spectrum to the reference spectrum of Fig. 1(b). For this result the "real data points" are indicated by the larger open circles separated from each other by 6.1 GHz, and the interpolated points obtained from the zero-padding are separated from each other by 0.61 GHz and define the solid line. The so called "real points" are for the frequency components obtained from the FFT of the original 165 ps scan. The weaker water lines appear with their expected frequencies, strengths and with linewidths equal to the spectral resolution of 6.1 GHz. The central frequency of the measured water lines was determined to an accuracy of ± 1 GHz as indicated on Fig. 2. The frequency in parenthesis is the accepted handbook value. Only water lines were observed.

III. Understanding the THz Pulse Reshaping of the Long-Tube Measurement

Obtaining the Refractivity $(n(\omega)-1)$ *of Water Vapor:* We will now obtain the absorption coefficient $\alpha(\omega)$ and the refrac-

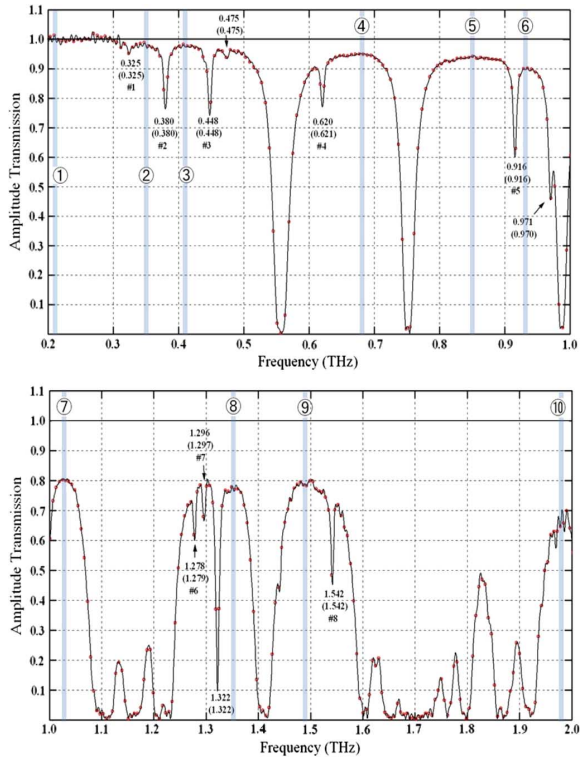

Fig. 2. Amplitude transmission through 6.18 m of atmosphere at 21 °C with RH 51%. 10 water windows (circled numbers) and 8 weak water lines are marked to compare with previous predictions and measurements. (Figure adapted from [1].)

tivity $(n(\omega)-1)$ of water vapor from the original sample and reference pulse measurements corresponding to Fig. 1(a). From the ratio of the complex Fourier transforms of the original data for the THz sample pulse with respect to the THz reference pulse shown in Fig. 1(a), we obtain the phase shifts of the water resonance lines as shown in Fig. 3. This phase data and the transmission measurement shown in Fig. 2 were fit to the causal absorption and phase shift lineshapes of the v-VW theory [4], [5], given below as

$$\alpha(\omega) = D \cdot \sum_j \frac{A_j}{\pi} \left(\frac{\omega}{\omega_j}\right)^2 \cdot \left[\frac{\Delta\omega_j}{(\omega-\omega_j)^2 + \left(\frac{\Delta\omega_j}{2}\right)^2} + \frac{\Delta\omega_j}{(\omega+\omega_j)^2 + \left(\frac{\Delta\omega_j}{2}\right)^2}\right] \tag{1}$$

where j refers to the water vapor resonance line ω_j. The corresponding change of the wave vector (phase) is given by

$$\Delta k(\omega) = D \cdot \sum_j 2\frac{A_j}{\pi\omega_j} \left(\frac{\omega\omega_j}{\omega_j^2-\omega^2}\right) \left[1 - \frac{\Delta\omega_j^2}{8\omega_j}\left(\frac{\omega}{\omega_j}\right) \cdot \left(\frac{\omega_j+\omega}{(\omega_j-\omega)^2 + \left(\frac{\Delta\omega_j}{2}\right)^2} - \frac{\omega_j-\omega}{(\omega_j+\omega)^2 + \left(\frac{\Delta\omega_j}{2}\right)^2}\right)\right] \tag{2}$$

for which

$$(n(\omega)-1) = \Delta k \lambda_o / 2\pi. \tag{3}$$

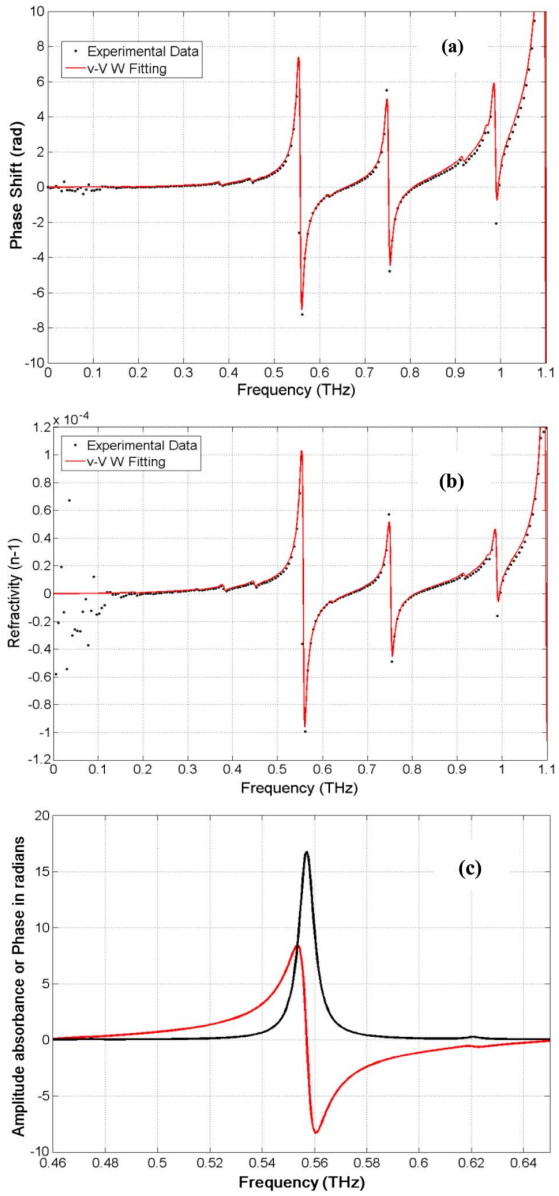

Fig. 3. (a) Calculated phase $\varphi = \Delta \mathrm{k} \mathrm{L}$ (solid line) and measured phase (dots) for transmission through 6.18 m of atmosphere at 21°C with RH 51% (water vapor density 9.3 g/m^3). (b) Refractivity $(n(\omega) - 1)$ obtained from Eq.(3) and the results of (a). (c) Relationship between the v-VW amplitude absorbance (upper curve) and the corresponding phase shift in radians (lower curve) for the experimental conditions of Fig. 3(a), These curves are identical with the same 7 GHz FWHM linewidth for all the ω_j lines, except for their strength A_j.

The A_j line-strength values are from the JPL data base [6], from which ω_j was summed up to 10 THz involving 1305 lines. It is important to note that reducing the frequency extent to 5 THz makes a significant change in the calculated phase from 0.1 to 1 THz shown in Fig. 3(a), but not the absorption as shown in Fig. 4. Another point is that the JPL database does not include the relatively weak, but observable water lines at 0.659 and 0.861 THz. Also, there is an oxygen line at 60 GHz and a weaker oxygen line at 118.7 GHz in the atmosphere. Both of the sums are multiplied by the factor D (explained in [4] and [5]), which is proportional to the density of water vapor in g/m^3; L is the distance in meters. For Figs. 3 and 4, $\mathrm{D} = 1.05 \times 10^6$, $\mathrm{L} = 6.18$ m, and the FWHM linewidth $\Delta\omega_j = 2\pi \times 7$ GHz for all of the ω_j lines.

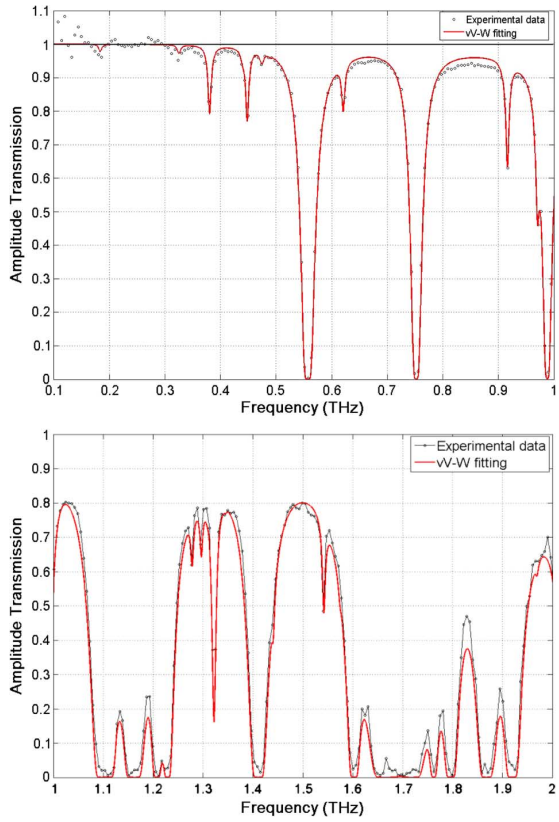

Fig. 4. v-VW amplitude transmission compared to the experimental measurements of Fig. 2.

In Fig. 3(a) the calculated phase $\varphi = \Delta \mathrm{k} \mathrm{L}$ shown as the solid line agrees quite well with the measured phase shown as the black dots. A measure of our accuracy is that the small phase shifts of the weak water lines are easily identified in the figure. The refractivity obtained from these results, using (3). is shown in Fig. 3(b). We note the relationship of this work to the earlier work at higher frequencies [7] and to the MPM propagation model of Liebe [8], [9]. It is also important to note the general relationship between the absorbance and phase for the corresponding causal v-VW lineshapes illustrated in Fig. 3(c).

In Fig. 4 the corresponding calculated transmission shown as the solid line agrees quite well with the measurement plotted as the same open circles shown in Fig. 2. The v-VW theory achieved the best fit with the FWHM linewidth of $\Delta\omega_j = 2\pi \times$ 7 GHz for all of the lines. It is important to understand, that our analysis has only three parameters, the amount of water vapor, the distance L and the linewidth. The accuracy of the results given above is acceptable for our initial calculations of pulse propagation with a path length of 6.18 m, but for much longer propagation distances of hundreds of meters, the discrepancy between the observed and calculated absorption in the windows of transparency (minimum absorption) below 1 THz can become a problem.

The phenomenon behind this problem is the poorly understood continuum absorption of water vapor, which is important in the transparent frequency regions, where the absorption due to the resonant lines of water vapor is a minimum.

From these self-consistent fits of the absorption coefficient $\alpha(\omega)$ and phase $\Delta \mathrm{k}(\omega)\mathrm{L}$ to the v-VW lineshapes, we calculate

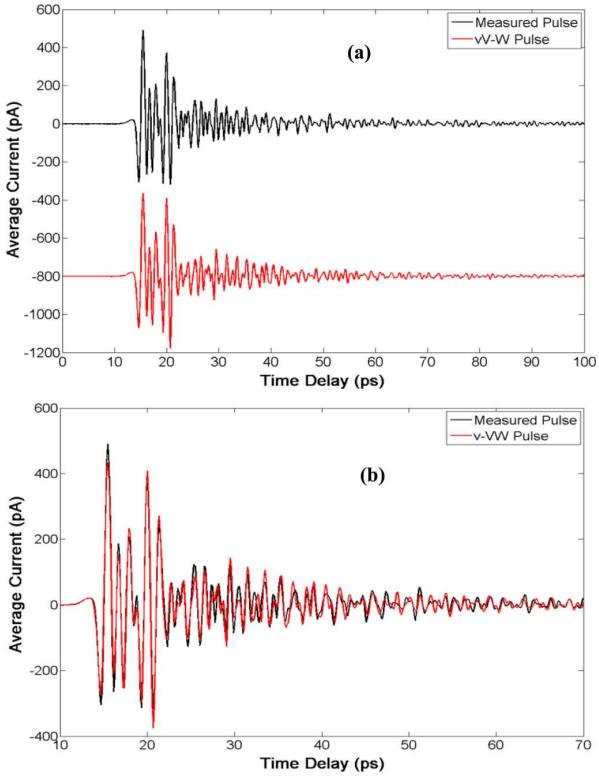

Fig. 5. (a) The upper measured transmitted THz pulse of Fig. 1(a) is compared to the lower calculated THz pulse with $z = 6.18$ m . . . (b) the measured and propagated pulses are overlapped for comparison.

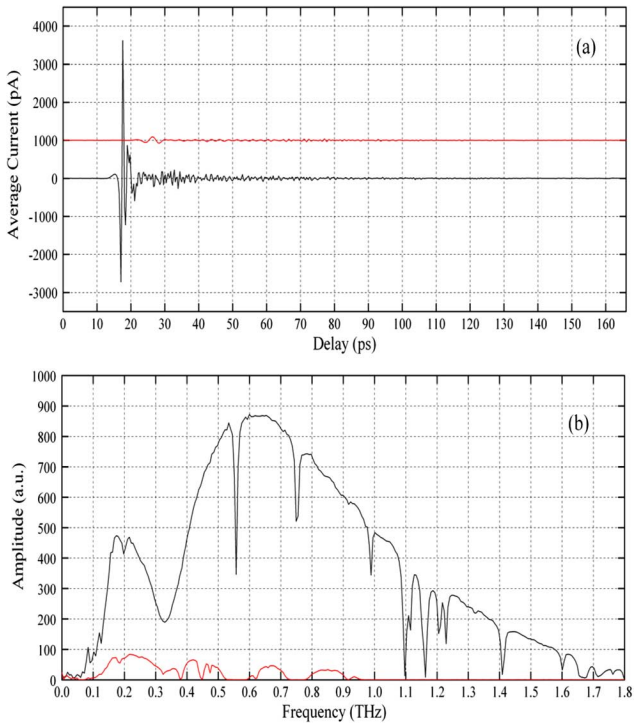

Fig. 6. (a) Measured THz input pulse (lower trace) and measured THz output pulse (upper trace) from the 167 m long-path with RH 51% at 21°C. (water vapor density 9.3 g/m^3). (b) Corresponding amplitude spectrum for THz input pulse (upper curve) and the amplitude spectrum of the output pulse (lower curve). Figure adapted from [2].

the frequency components of the transmitted pulse through the water vapor in the sample chamber, using the complex Fourier transform of the reference pulse E(0, ω), as follows:

$$E(z,\omega) = E(0,\omega)exp\left[i\Delta k(\omega)z\right]exp\left[-\alpha(\omega)z/2\right]. \quad (4)$$

Then the corresponding THz output pulse is obtained by taking the inverse numerical Fourier transform (IFFT) of the output frequency components, as given by (4). Our results are shown in Fig. 5(a) for the measured pulse in Fig. 1(a) and the calculated pulse. These are shown overlapped in Fig. 5(b) to indicate the good agreement between the two results, for which the pulse modulations are quite similar with small differences in amplitude.

IV. Discussion of the Previous Long-Path Measurements

We now describe the previous investigation of the limits of short, broadband THz pulse propagation in the atmosphere using the same low-power, high signal-to-noise ratio (S/N) coherent optoelectronic system [2]. We will use these measurements to provide the input experimental pulses for our long path calculations, and to provide realistic S/N ratios for the calculated long path pulses. For this experiment a 30 nW average power beam of 0.5 ps THz pulses was transmitted through the atmosphere a distance of 167 m and the transmitted pulses with an average power of 130 pW were measured and compared to the input pulses, using the THz-TDS technique.

Using collimating, focusing and flat mirrors, it was possible to direct a relatively large fraction of the THz radiation onto a distant target. The burst of THz radiation emitted by the transmitter was collimated by the THz optical system into a diffraction-limited beam, which was coupled into the long-path system and returned with good coupling efficiency into the THz receiver. The resulting tightly coupled system of the THz transmitter and receiver (transceiver) gave strong reception of the incoming THz pulses with 130 pW average power.

The coupling efficiency is almost diffraction limited at the 200 GHz spectral peak of the return beam. The initial collimated Gaussian beam diameter of 30 cm expands to 126 cm after propagating 161 m to return to the 30 cm diameter focusing mirror. The returning spectral amplitude at 0.2 THz is reduced by the ratio $30/126 = 0.24$ of these diameters. In addition, the amplitude transmission for this propagation length due to the water vapor absorption was 0.95. Assuming 100% coupling to the THz receiver, the total amplitude reduction would be $0.24 \times 0.95 = 0.23$, compared to the measured ratio of 0.19 from Figs. 6(b) and 7(b), indicating that the amplitude coupling to the receiver was 83%.

The data taking and processing was similar to that described in Section II. Fig. 6(a) compares the averaged input pulse to the averaged output pulse. The input pulse appears quite clean with little oscillation due to the much smaller 50 cm path in the atmosphere. When the input pulse was coupled to the long 167 m path in laboratory air with RH 51% at 21 °C, the output pulse showed very strong and extended ringing from the rotational

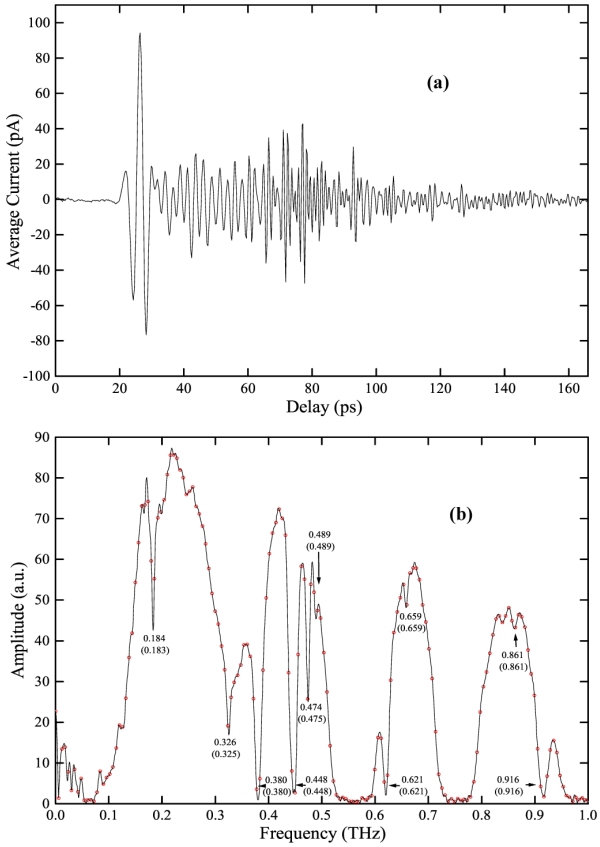

Fig. 7. (a) Expanded vertical scale view of the measured output pulse of Fig. 6(a). (b) Expanded vertical scale view of the amplitude output spectrum of Fig. 6(b). The "real data points" are indicated by the open circles, separated from each other by 6.1 GHz; zero-padding defines the solid line. Figure adapted from [2].

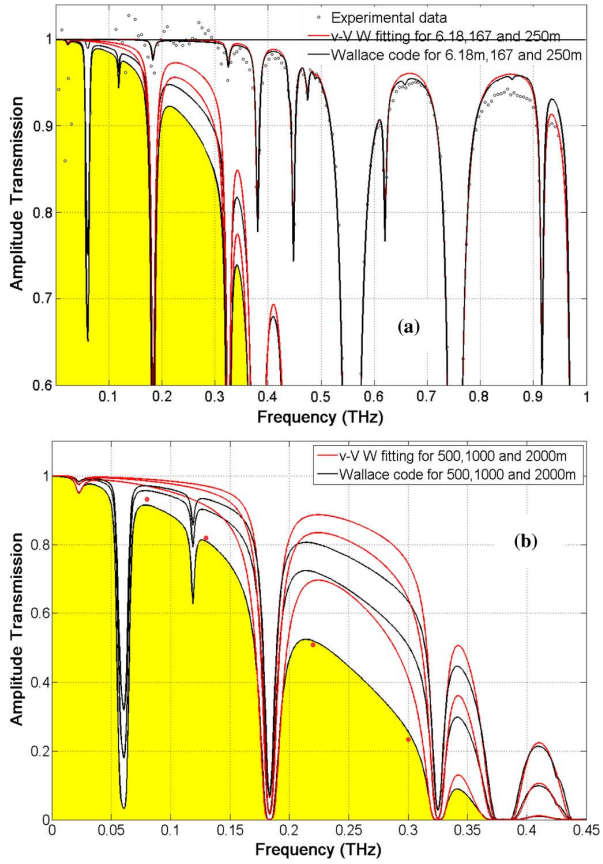

Fig. 8. (a) The calculated amplitude transmission through 6.18 m, 167 m and 250 m of atmosphere at 21°C and RH 51% together with the experimental "real point" data for 6.18 m from Fig. 2. The v-VW calculation is the upper (red) curve and the Wallace code result is the lower (black) curve. (b) The calculated amplitude transmission from 0 to 0.45 THz through 500 m, 1000 m and 2000 m of atmosphere at 21°C and RH 51%.

lines of water vapor in Fig. 7(a), with an expanded vertical scale compared to Fig. 6(a).

The comparison of the averaged input and averaged output amplitude spectra is shown in Fig. 6(b). The input spectrum shows the well resolved unsaturated strong water lines, due to the much shorter 50 cm path in the THz-TDS system. In contrast, the output spectrum for the 167 m path shows complete absorption bands for the saturated strong water lines and the significant appearance of the very weak water lines. Fig. 7(b) shows (with an expanded vertical scale) the amplitude spectrum of the long-path pulse with the weak water lines clearly displayed and identified to a precision of 1 GHz, with the resolution-limited linewidths of 6.1 GHz. The transmission of the spectral windows between the strong water lines illustrates the THz potential for ranging, imaging, communications and sensing of vapors in the range of a few hundred meters [3], [10], [11].

A careful study of the transmitted THz pulses through 167 m of humid air revealed a promising THz bit pulse for digital (binary) communications [2]. As shown in Fig. 7(a), the almost separated initial low-frequency pulse of the frequency swept and broadened transmitted pulse, appears to be propagating with little loss and distortion.

One can understand the formation and separation of the THz bit pulse as follows [2]: "The initial optical excitation pulse of the transmitter generates the initial short input THz pulse with all of the corresponding frequency components of the input amplitude spectrum in phase. During propagation through the long-path of the atmosphere, the higher frequency components are much more attenuated and have significantly slower speeds. Consequently, the frequencies separate during their passage through the atmospheric path of 167 m with the higher frequencies extending the pulse train. The initial 0.5 ps input pulse changes into a ringing, frequency swept, output pulse extending to as much as 160 ps with the highest frequency at the end of the pulse. In addition, the higher frequencies are much more attenuated by the water vapor. The lowest frequency components appear together at the front of the output pulse with very little attenuation and broadening."

To provide a test of the simple proposal that the lower frequency THz components would keep their initial phase coherence, while propagating through the 167 m long-path, the predicted output pulse was numerically calculated (IFFT) from the output amplitude spectrum between 0.07 and 0.37 THz with all of the frequency components in phase. The calculated phase coherent output pulse was compared to the experimentally observed THz bit pulse on the leading edge of the output pulse. The similarity of the two pulses confirmed the coherent and stable THz bit pulseshape for the 167 m propagation distance and predicted stability for longer distances.

V. Calculation of Long-Path THz Pulses

Now, using the analysis presented in (1)–(4), it has become possible to test the range of the THz bit pulse and its predicted emergence from the complicated wide bandwidth pulse at 167 m. In order to first gain some insight into the expected absorption, we plot in Fig. 8(a), the calculated amplitude transmission for the 6.18 m path of Figs. 2 and 4, the 167 m path of Figs. 6 and 7, and a 250 m long-path, all at 21 °C and RH 51% (water vapor density 9.3 g/m^3). Here, we compare the results from (1) with $\Delta\omega_j = 2\pi \times 7$ GHz for all of the ω_j lines, with the more sophisticated calculation of H.B. Wallace, responsible for Fig. 3 in [11]. The Wallace curve includes the poorly understood continuum absorption of water vapor, which can be the dominant absorption in the low frequency windows of transparency of water vapor. It also includes the two weak water lines at 0.659 and 0.861 THz, and the relatively strong and weak oxygen lines at 60 and 118.7 GHz, respectively. We note that the Wallace calculation is closely related to the work of Liebe [8], [9].

In Fig. 8(a) the v-VW and Wallace calculations look quite similar for the 6.18 m path, but show the effect of including the continuum absorption in the much longer 167 m path and the 250 m path. In Fig. 8(b) the two calculations are compared from 0.0 to 0.45 THz for the much longer paths of 500, 1000, and 2000 m. The red dots at 0.08, 0.13, 0.22, and 0.3 THz are taken from the recent experimental measurements and numerical fitting of the absorption of the water vapor continuum [12]. The yellow highlight indicates the predicted Wallace code (black lines) amplitude transmission at 250 m [Fig. 8(a)] and 2000 m [Fig. 8(b)]. The v-VW calculation predicts the higher transmission indicated by the red lines. For frequencies below 0.3 THz, it is not possible to decrease the van-Vleck Weisskopf transmission to that of the Wallace curve by simply increasing the linewidth. For example, with a linewidth of 12 GHz, the v-VW transmission is still above that of the Wallace curve, while such a broad linewidth destroys the acceptable agreement at higher frequencies.

Fig. 9 shows the data set from a recent experiment for a 137 m path with relatively good system stability for measurements at 21°C and RH 10.5% and RH 46.5%. These two measurements were used to test the accuracy of the much longer path calculated output pulses, as shown in Fig. 9(a). The top trace is the measured output pulse at RH 10.5%, and the trace underneath is the measured THz output pulse with RH 46.5%. The complex numerical Fourier transform of the RH 10.5% pulse provides the input spectrum to the two numerical propagation calculations, one using the hybrid Wallace absorption with v-VW phase ((2)) and other using the pure v-VW absorption and phase of (1) and (2). The hybrid Wallace approach was needed, because the Wallace code only gives absorption. The numerical Fourier transforms of both frequency-domain calculations using (4) are compared with the RH 46.5% output pulse in Fig. 9(a). The output pulses from both calculations show good agreement with each other and the experiment. Consequently, we can extend our calculations to longer lengths with reasonable confidence in their tested accuracy.

We will now test the predicted range of the THz bit pulse and its emergence from the complicated wide bandwidth pulse at 167 m [2]. In order to do this, the ringing frequency swept output

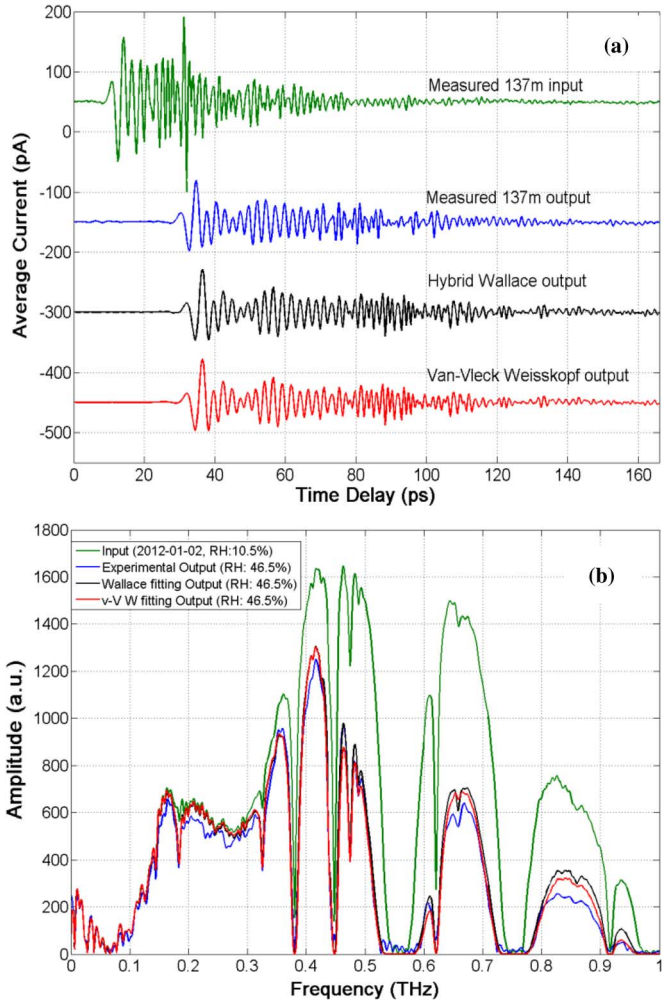

Fig. 9. (a) Measured output pulse for 21 °C, RH 10.5% and 1.9 g/m^3 (input pulse), and the measured output pulse for 21 °C, RH 46.5% and 8.5 g/m^3. Corresponding calculated output pulse using the RH 10.5% pulse as input and calculating the propagation through 137 m at RH (46.5%–10.5%), using the hybrid Wallace calculation or the pure v-VW calculation. (b) Corresponding amplitude spectra.

pulse of Fig. 7(a) is taken to be the input pulse to the longer path lengths of 100 and 200 m at RH 51% at 21 °C. These calculations assume perfect coupling and use the absorption and dispersion (phase) given by (1) and (2). The consequent THz output pulses are shown in Fig. 10(a), together with the 167 m THz pulse, used as the input pulse to the calculation. The THz bit pulseshape changes and broadens with the additional propagation, while the higher frequency ringing is significantly attenuated. However, it remains clear that the THz bit pulse structure is capable of digital transmission for distances of the order of 300 m.

Fig. 11(a) presents much longer path propagation results, where the 167 m output pulse was again used as the input pulse to the calculations. The top trace shows the 167 m input pulse together with the additional path lengths of 500, 1000, and 2000 m at RH 51% at 21 °C. Fig. 11(b) shows the corresponding amplitude spectra. The important similarity shown in the transmitted pulses for 500, 1000, and 2000 m in Figs. 11(a) and 13(a) and also in the transmitted spectra of Figs. 11(b) and 13(b) shows the emergence and overlapping of two new THz bit pulses I and II, which will be discussed in detail later.

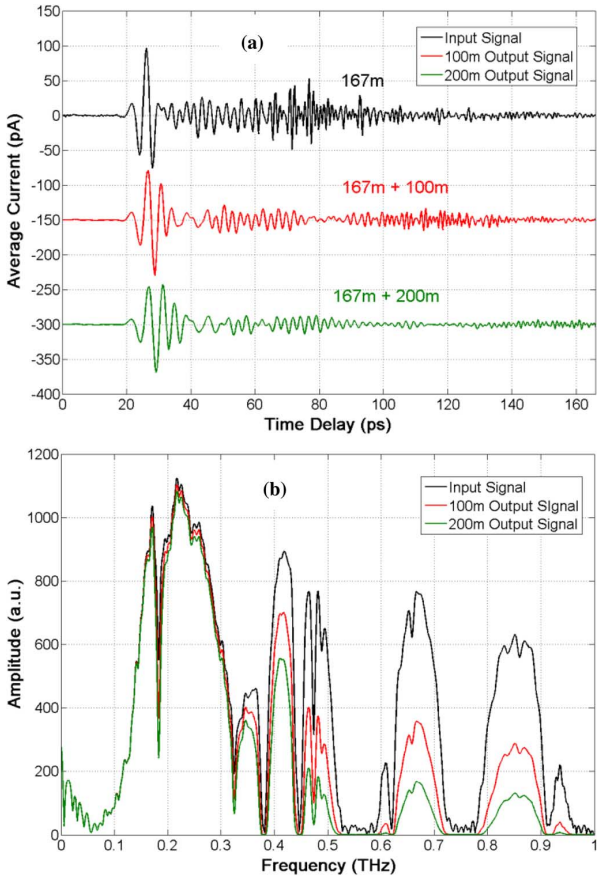

Fig. 10. (a) Input pulse is the 167 m pulse shown in Fig. 7(a). The 167 m + 100 m pulse shows the v-VW propagated pulses after 100 m, and the 167 m + 200 m pulse after 200 m of calculated propagation. (b) Corresponding amplitude spectra.

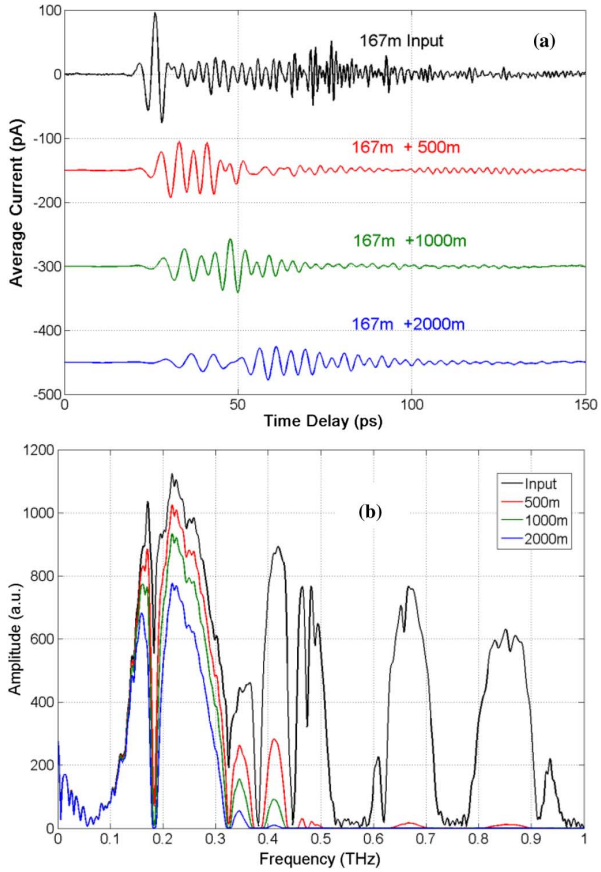

Fig. 11. (a) Input pulse (167 m pulse of Fig. 7(a). Input pulse after 500, 1000, and 2000 m of v-VW calculated propagation. (b) Corresponding amplitude spectra.

It is noteworthy that the predicted pulses are within the sensitivity range of our coherent system. A realistic estimate of the actual signal strength that would come back to the receiver is based on the simple expansion of a spherical wave. This additional attenuation factor of the amplitude spectrum is simply the ratio of $167\ \mathrm{m}/(167+L)$, where L is the additional pathlength. Correspondingly the attenuation factors are 0.250, 0.143, 0.077 for the additional path lengths of 500, 1000 and 2000 m, respectively. For the measured input pulse the signal to noise ratio is 200, indicating a receiver sensitivity of 1 pA. The peak-to-peak signal of the 2000 m signal is 50 pA and after multiplication by the spherical wave factor is 3.8 pA, which would be observable with a S/N ratio of 4.

As an additional check on the results of Fig. 11, the corresponding 167 m + 2000 m output pulse (hybrid Wallace) is compared to the v-VW pulse on an expanded vertical scale in Fig. 12(a), and the corresponding amplitude spectra are compared in Fig. 12(b). The impressive agreement between the two pulses in their oscillation structure shows the importance of the phase term. The disagreement in amplitude is simply explained by their respective amplitude spectra showing the higher Wallace absorption.

Fig. 13 shows the predicted THz bit pulse [2] as a function of the extra propagation length at RH 51% at 21 °C. The spectrum of the THz bit pulse was cut from the spectrum of the 167 m output pulse as shown in Fig. 13(b). Then, the entire spectrum was assumed to be in-phase at the start of the additional pathlength. The corresponding starting pulse is the top trace shown in Fig. 13(a) and shows by its symmetry that all of the frequency components are in-phase. This pulse is the same as the THz bit pulse shown in Fig. 10 of [2]. The changing pulseshape is shown in Fig. 13(a) as a function of the propagation distance.

The results in Fig. 13 show that during the propagation of the THz-bit pulse [2], the pulse appears to be separating into two independent pulses. A successful test of this concept is shown in Fig. 14 for which the original THz bit pulse [2], is considered to be the overlap of THz bit pulse I and THz bit pulse II. The natural boundary of the water line at 0.184 THz separates the spectra of the two pulses, and the natural boundary of the water line at 0.326 THz defines the high frequency boundary of pulse II. The low-frequency boundary of pulse I at 0.13 THz is determined by the spectral response of the THz receiver, slightly above the weak oxygen line at 0.12 THz.

THz bit pulse I is the coherent pulse shown in Fig. 14(a) with the amplitude spectrum indicated in Fig. 14(c). THz bit pulse II is the coherent pulse shown in Fig. 14(b) with the corresponding amplitude spectrum shown in Fig. 14(c). The long-path v-VW numerical propagation of these pulses is shown in Fig. 14(a) and 14(b), where it is seen that these pulses propagate with a

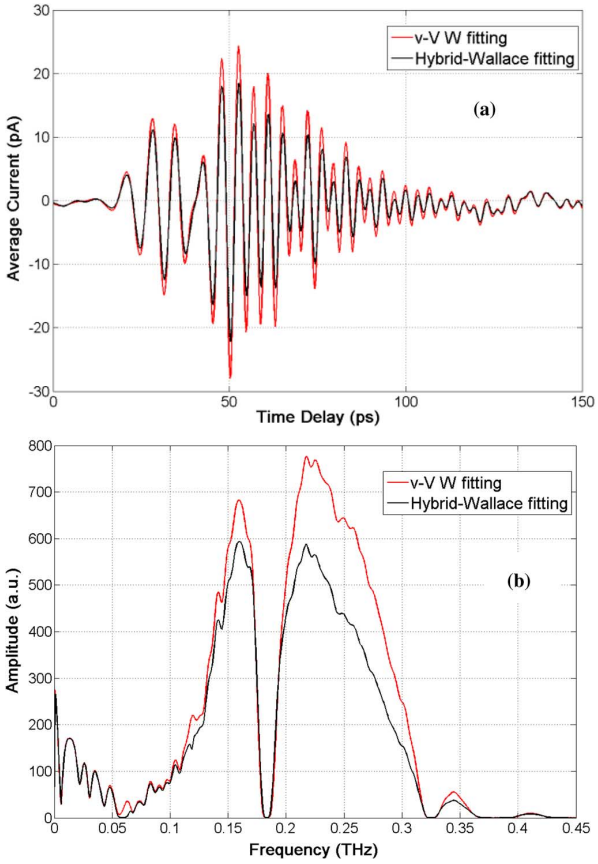

Fig. 12. (a) Comparison of the calculated 167 m + 2000 m output pulses of (hybrid-Wallace) and (pure v-VW). (b) Corresponding amplitude spectra.

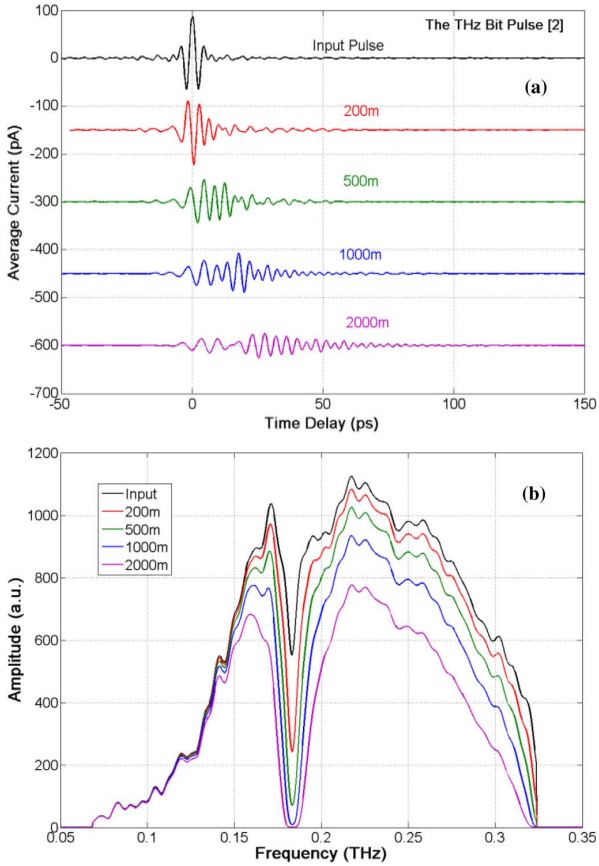

Fig. 13. (a) Calculated v-VW propagation of the phase coherent THz-bit pulse [2], with the corresponding amplitude spectrum shown in (b). High frequency boundary at 0.326 THz is the center of the water line.

relatively small amount of broadening and attenuation up to the impressive distance of 2 km.

From the propagation results shown in Fig. 14(a) for the THz-bit pulse-1, it is reasonable to consider a bit stream of these pulses separated from each other by 100 ps, corresponding to the bit rate of 10 Gb/s. From the propagation distance of 2 km, we obtain the bit rate distance product of 20 (Gb/s)-km. Similarly, for the propagation results shown in Fig. 14(b) for the THz bit pulse 2, consider a bit stream of these pulses separated from each other by 50 ps, corresponding to the bit rate of 20 Gb/s. Given the propagation distance of 2 km, we obtain the bit rate distance product of 40 (Gb/s)·km for 21 °C at RH 51% with 9.3 g/m^3 water vapor density. These values are competitive with optical fiber communications channels [13], [14], and show the potential for THz communications.

The bit rate distance products are dependent on weather conditions. Referring to Fig. 3 in [11], for winter conditions with −10 °C at RH 30% and water vapor density of 0.6 g/m^3, the propagation distance can be increased 30 km with similar propagation results, thereby giving the corresponding products of 300 and 600 (Gb/s)·km. However, for conditions of rain at 20°C and RH 44%, the propagation distance must be reduced to 500 m, giving the corresponding products of 5 and 10 (Gb/s)·km. For Fog and dust at 20 °C and RH 44%, the propagation distance must be reduced to 400 m, giving the corresponding products of 4 and 8 (Gb/s)·km.

VI. Discussion and Summary

We have extracted the measured refractivity of water vapor $(n(\omega) - 1)$ by analyzing the complex spectra from the original data of the precise coherent THz-TDS absorption measurement for a 6.18 m long sample path of the atmosphere [1]. The excellent fit of the new refractivity measurement and the previous absorption to the sum of the effects from all of the water vapor lines in the JPL data base from 0 to 10 THz [6], showed the precision and self-consistency of the original THz-TDS data. The consequent precision of the resulting numerically calculated analytic absorption coefficient $\alpha(\omega)$ and refractivity $(n(\omega)-1)$, for which all of the lines had the same van-Vleck Weisskopf lineshape with the FWHM linewidth of 7 GHz, and strengths from the JPL database, were demonstrated by the excellent agreement between the calculated output pulse after 6.18 m of atmospheric propagation and the measured output pulse, both using the same input pulse. The accuracy of $\alpha(\omega)$ and $(n(\omega) - 1)$ was also tested and proven to be excellent by comparison with new 137 m long-path propagation measurements.

Based on the demonstrated accuracy of the of $\alpha(\omega)$ and $(n(\omega) - 1)$ calculations, the THz output pulses for a variety of input pulses with the propagation distances of 500, 1000, and 2000 m have been calculated. The predicted stable propagation of the previously proposed "ideal THz bit pulse" [2] was tested and showed that this pulse evolves into two overlapping

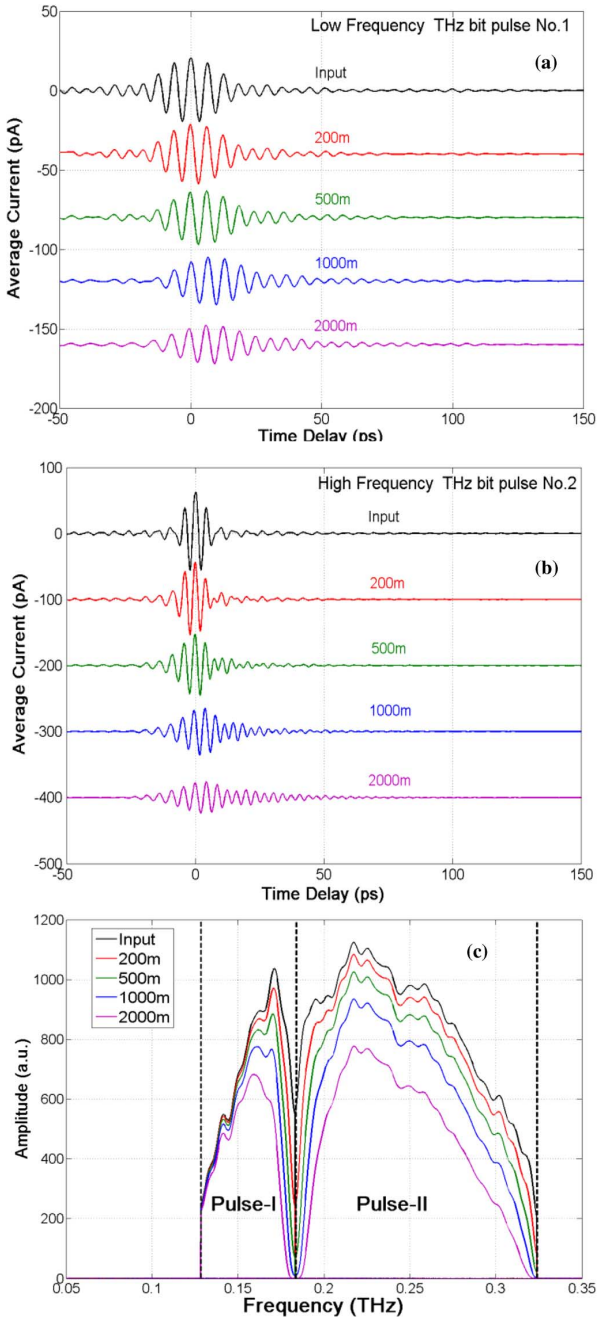

Fig. 14. (a) Calculated v-VW propagation of the low-frequency THz-bit pulse I. (b) Propagation of the High-Frequency THz-bit pulse II. (c) Amplitude spectra of the THz-bit pulses I and II. Indicated low frequency boundary is 0.128 THz. The central dividing boundary is defined by the water line at 0.184 THz, and the high frequency boundary is at the water line at 0.326 THz.

THz bit pulses after 1000 m of propagation. These transform limited THz bit pulses I and II span the spectral ranges of 0.13–0.18 THz and 0.18–0.33 THz, respectively. These two pulses were shown to have pulse stability with propagation of up to 2 km, and can support the bit rate distance products of 20 and 40 (Gb/s)·km, respectively. These bit rate distance products are competitive with optical fiber digital communications channels, and clearly show the potential for many applications.

ACKNOWLEDGMENT

The authors thank H. B. Wallace for allowing them to use his computer program, which includes the water vapor continuum, the weak water lines and low frequency oxygen lines, to calculate the absorption of the atmosphere from very low frequencies up 1.0 THz.

REFERENCES

[1] Y. Yang, A. Shutler, and D. Grischkowsky, "Measurement of the transmission of the atmosphere from 0.2 to 2 THz," *Opt. Express*, vol. 19, pp. 8830–8838, 2011.

[2] Y. Yang, M. Mandehgar, and D. R. Grischkowsky, "Broad-band THz pulse transmission through the atmosphere," *IEEE Trans. THz Sci. Technol.*, vol. 1, no. 1, pp. 264–273, Sep. 2011.

[3] J. S. Melinger, Y. Yang, M. Mandehgar, and D. Grischkowsky, "THz detection of small molecule vapors in the atmospheric transmission windows," *Opt. Express*, vol. 20, pp. 6788–6807, 2012.

[4] C. H. Townes and A. L. Schawlow, *Microwave Spectroscopy*. New York: Dover, 1975.

[5] H. Harde, R. A. Cheville, and D. Grischkowsky, "THz studies of collision broadened rotational lines," *J. Phys. Chem. A*, vol. 101, pp. 3646–3660, 1997.

[6] H. M. Pickett, R. L. Poynter, E. A. Cohen, M. L. Delitsky, J. C. Pearson, and H. S. P. Muller, "Sub-millimeter, millimeter, and microwave spectral line catalog," *JQSRT* vol. 60, pp. 883–890, 1998 [Online]. Available: http://spec.jpl.nasa.gov/

[7] R. F. Calfee, "Anomalous dispersion calculated for atmospheric water vapor," *Appl. Opt.*, vol. 7, pp. 1652–1654, 1968.

[8] H. J. Liebe, "An updated model for millimeter wave propagation in moist air," *Radio Sci.*, vol. 20, pp. 1069–1089, 1985.

[9] H. J. Liebe, *MPM-An Atmospheric Millimeter-Wave Propagation Model*, vol. 10, pp. 631–650, 1989.

[10] P. H. Siegel, "Terahertz technology," *IEEE Trans. Microw. Theory Techn.*, vol. 50, no. , pp. 910–928, 2002.

[11] R. Appleby and H. B. Wallace, "Standoff detection of weapons and contraband in the 100 GHz to 1 THz region," *IEEE Trans. Antennas Propag.*, vol. 55, no. 11, pp. 2944–2956, Nov. 2007.

[12] V. V. Podobedov, D. F. Plusquellic, K. E. Siegrist, G. T. Fraser, Q. Ma, and R. H. Tipping, "New measurements of the water vapor continuum in the region from 0.3 to 2.7 THz," *J. Quantit. Spectrosc. Radiative Transfer*, vol. 109, pp. 458–467, 2008.

[13] A. Kawana, M. Kawachi, T. Miyashita, M. Saruwateri, K. Asatani, J. Yamada, and K. Oe, "Pulse broadening in long-span single-mode fibers around a material-dispersion-free wavelength," *Opt. Lett.*, vol. 2, pp. 106–108, 1978.

[14] G. P. Agrawal, *Fiber-Optic Communication Systems*, 4th ed. Hoboken, NJ: Wiley, 2010.

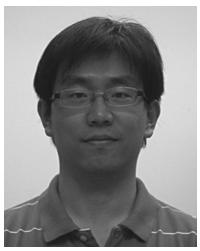

Yihong Yang (S'11) was born in Hebei, China, in 1983. He received the B.S. and M.S. degrees from Nankai University, Tianjin, China, in 2006, and 2009, respectively, and is currently working toward the Ph.D. degree in the School of Electrical and Computer Engineering, Oklahoma State University, Stillwater.

His current research interests include terahertz time-domain detection, broadband terahertz atmosphere propagation, and terahertz communication.

Mahboubeh Mandehgar received the B.S. degree from Azzahra University, Tehran, Iran, in 2003 and the M.S. degree from University of Central Missouri, in 2010, and is currently working toward the Ph.D. degree on THz spectroscopy and THz communication system.

Daniel R. Grischkowsky (SM'90–F'92) received the B.S. degree from Oregon State University, Corvallis, OR, in 1962, and the Ph.D. degree from Columbia University, New York, in 1968.

In 1969, he joined the IBM Watson Research Center, Yorktown Heights, NY. In 1993, he joined Oklahoma State University, where his work has concentrated on unique applications of THz-TDS, including waveguides, the Sommerfeld wave, surface waves, hole arrays and photonic crystals.

Dr. Grischkowsky is a Fellow of the Optical Society of America (OSA) and the American Physical Society. He was awarded the 1985 Boris Pregel Award by the NY Academy of Sciences, the OSA 1989 R. W. Wood Prize, the OSA 2003 William F. Meggers Award, and the 2011 Kenneth J. Button Prize from the International Society of IR, MM and THz waves.